



Gold particle size effect in biomass-derived lignan hydroxymatairesinol oxidation over Au/Al₂O₃ catalysts



Martín López^a, Olga A. Simakova^b, Elena V. Murzina^b, Stefan M. Willför^c, Igor Prosvirin^d, Andrey Simakov^e, Dmitry Yu. Murzin^{b,*}

^a Posgrado de Ciencia e Ingeniería de Materiales de la UNAM, Centro de Nanociencias y Nanotecnología, C.P. 22860, Ensenada, Baja California, Mexico

^b Laboratory of Industrial Chemistry and Reaction Engineering, Process Chemistry Centre, Åbo Akademi University, FI-20500 Åbo/Turku, Finland

^c Laboratory of Wood and Paper Chemistry, Process Chemistry Centre, Åbo Akademi University, FI-20500 Åbo/Turku, Finland

^d Boreskov Institute of Catalysis, Lavrentieva 5, Novosibirsk 630090, Russia

^e Universidad Nacional Autónoma de México, Centro de Nanociencias y Nanotecnología, km. 107 Carretera Tijuana-Ensenada, C.P. 22860, Ensenada, Baja California, Mexico

ARTICLE INFO

Article history:

Received 15 September 2014

Received in revised form

28 December 2014

Accepted 29 December 2014

Available online 6 January 2015

Keywords:

Sol-gel

UV-visible spectroscopy

Oxomatairesinol (oxoMAT)

Structure sensitivity

ABSTRACT

The heterogeneously catalyzed aerobic selective oxidation of naturally occurring lignan hydroxymatairesinol (HMR) to another lignan oxomatairesinol (oxoMAT) was carried out at 70 °C and atmospheric pressure over gold nanoparticles with different sizes supported on alumina prepared from organometallic precursor by the sol-gel method. Precursor of gold nanoparticles (i.e. gold hydroxide) was supported on alumina by deposition-precipitation with urea from HAuCl₄ aqueous solution followed by washing with ammonium hydroxide. The size of the supported gold nanoparticles was changed by either treatment under hydrogen flow at different temperatures or exposure to ultraviolet (UV) irradiation at the wavelength of 254 nm. The catalysts were characterized by inductively coupled plasma atomic emission spectroscopy (ICP-AES), nitrogen adsorption, X-ray diffraction (XRD), transmission electron microscopy (TEM), X-ray photoelectron spectra (XPS), and UV-visible spectroscopy (UV-vis). Structure sensitivity in HMR oxidation was studied showing that the reaction rate passes through a maximum when the gold cluster size is ca. 4 nm.

© 2015 Elsevier B.V. All rights reserved.

1. Introduction

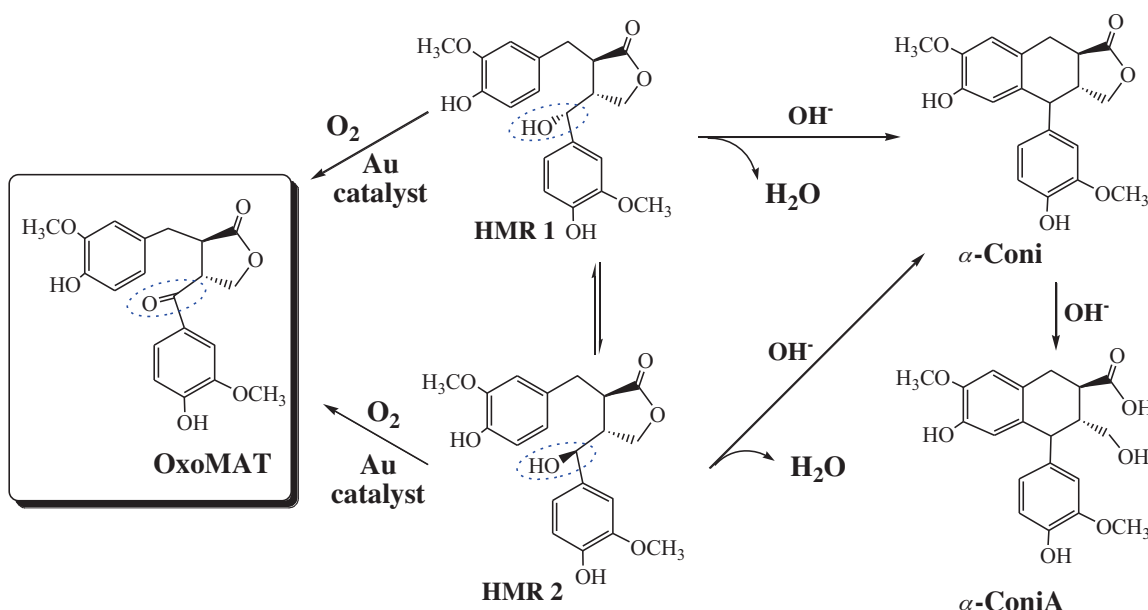
Catalysis using gold nanoparticles recently became attractive for many researches since the moment when Haruta and Hutchings independently and almost simultaneously in around 1987 discovered that gold served as an extraordinary good heterogeneous catalyst in the low-temperature oxidation of CO and the hydrochlorination of ethyne to vinyl chloride, respectively [1–3]. Nowadays gold catalysts are well known for being highly active and selective in different oxidation reactions, in particular, transformations of alcohols to corresponding aldehydes, ketones and acids [4–9]. These reactions are among the fundamental ones in biomass catalytic conversion.

Wood biomass offers a wide range of possibilities from the view point of biosustainable chemical processes. It can be transformed not only into fuels and basic chemicals, but also into fine

chemicals. Biomass derived extractives can be found mainly in knots and bark, which are normally considered to be a waste in pulp and paper industry. Lignans are a group of phenolic compounds found in different parts of plants, while the richest source is knot wood. For example, Norway spruce (*Picea abies*) knots contain a large amount of lignans including hydroxymatairesinol (HMR), which is the most abundant, constituting 65–85 wt.% of the lignans. Lignans having anticarcinogenic and antioxidative effects can be applied for the cosmetic (skin- and hair-care products) and pharmaceutical use. Thus, the lignan oxomatairesinol (oxoMAT), which is valuable for such applications, can be synthesized via dehydrogenation/oxidation of secondary alcohol group present in HMR (Scheme 1).

The formation of oxoMAT from HMR by light-irradiation was reported in [10], while in [11] 2,3-dichloro-5,6-dicyano-1,4-benzoquinone (DDQ) was used as an oxidizing agent. Hence a need for industrially applicable catalytic methods for the selective synthesis of lignan oxoMAT exists. Commercially more attractive heterogeneously catalyzed synthesis of oxoMAT was performed over supported palladium [12] and gold catalysts [13,14]. The

* Corresponding author. Tel.: +358 22154985.
E-mail address: dmurzin@abo.fi (D.Yu. Murzin).



Scheme 1. Transformations of the lignan hydroxymatairesinol (HMR) over gold catalysts.

former studies demonstrated superior performance of gold catalysts over palladium ones in terms of activity and selectivity. Moreover, utilization of gold catalysts allowed carrying out the reaction under environmentally benign conditions, using oxygen from air as an oxidant, water-alcohol mixture as a solvent and low temperature. Therefore, further investigation of the reaction became focused on application of the heterogeneous gold catalysts, in particular Au/Al_2O_3 .

It is generally accepted, that catalytic activity of gold catalysts is strongly dependent on gold particle size [15]. In [16,17] it was pointed out that the largest effect on the activity is attributed to the presence of low-coordinated Au atoms, which are abundant on the smallest gold nanoparticles. The most reactive atoms are located at the edges and corners of particles. These Au atoms are suggested to be able to facilitate adsorption of CO and dioxygen to perform CO oxidation reaction. The number of low-coordinated corner and edges sites is decreasing with increasing of Au particle size. Therefore, even the particle size changing slightly, the fraction of active sites decreases dramatically. The other effects, such as interactions with the support [18,19], charge transfer [20], strain [21] were suggested to contribute, albeit to a lesser extent. Gold catalysts are known to exhibit structure sensitivity in particular in hydrogenation reactions [22]; oxidation of CO [23], glycerol [24], alcohols [25] and sugars [26,27].

The aim of the present work was to investigate the structure sensitivity of the biomass-derived lignan HMR oxidative dehydrogenation on the Au nanoparticles (NPs) supported on alumina. Recently it was reported that oxidation of HMR over Au NPs supported on the commercially available γ -alumina demonstrated volcano-shape relationship between the reaction rate and the size of Au particles with the maximum at around 2 nm [28]. In [14] it was found that alumina prepared by the sol-gel method possesses appropriate acidity for improving activity of gold catalysts in the selective oxidation of HMR. Since both, support acidity and Au particle size, impact the reaction rate it is important to investigate the effect of the gold particle size in the case of a more acidic catalyst support. Therefore, in the current work sol-gel alumina prepared with an organo-metallic precursor was used bearing enhanced acid properties as was already demonstrated in our previous work [14].

2. Experimental

2.1. Catalyst preparation

Alumina support was prepared by a sol-gel method from a metallo-organic precursor following a procedure reported previously [29]. 75 mL of aluminum sec-butoxide (Alfa-Aesar) were mixed with 50 mL of 2-methyl-2,4-pentanediol (Alfa-Aesar), staying in reflux for 3 h, with moderate agitation at 80 °C. Hydrolysis was performed by drop wise adding of 50 mL of deionized water. The obtained gel was aged for 10 h. The sample was dried under vacuum (about 10^{-3} Torr) at 100 °C for 12 h and then heated in N_2 atmosphere at 450 °C for 12 h with a ramp rate 5 °C/min, followed by treatment in O_2 at 650 °C for 4 h for decomposition of organic residuals.

Gold (1 wt.%) was supported by deposition-precipitation using urea as a precipitation agent. 4 g of prepared alumina support were added to 400 ml of aqueous solution of $HAuCl_4$ (4.2×10^{-3} M) and urea (0.42 M). The initial pH of solution was ca. 2. After vigorous stirring at 80 °C for 4 h the suspension was filtered and washed with ammonium hydroxide (25 M) for 30 min. The pH of the solution after stirring with ammonium hydroxide was ca. 10. Finally, the sample was washed in water until pH was 7, filtered and dried at room temperature for 24 h. The obtained catalyst was denoted as Au/Al_2O_3 -F.

In order to form gold nanoparticles (Au NPs) with different sizes certain amounts of freshly prepared Au/Al_2O_3 -F were treated in hydrogen flow at different temperatures or exposed to ultraviolet (UV) irradiation at 254 nm, using a fully microprocessor controlled unit UVlink CL 508 Crosslinker (Uvitec Cambridge) equipped with an integrating sphere. Temperature programmed reduction (TPR) of freshly prepared gold samples was carried out in a flow reactor under linear sample heating with ramp 20 °C/min up to 250, 350 and 600 °C using gas mixture 3 vol.% H_2 in He.

2.2. Catalyst characterization

Chemical analysis for obtained gold samples was done with an inductively coupled plasma atomic emission spectroscopy (ICP-AES) using ICP Liberty 110 Emission Spectrometer Varian. For each

measurement 30 mg of sample was dissolved in the 20 ml of acids mixture ($\text{H}_2\text{SO}_4:\text{HCl}:\text{HNO}_3 = 6:6:3$) and heated up to 150 °C.

The specific surface area and pore size distribution were determined by nitrogen adsorption measurements in a Tri-Star III device applying BET method. Before analysis the samples were treated in a vacuum (10^{-3} Torr) at 300 °C for 4 h.

X-ray diffraction (XRD) analysis was carried out by Philips X'pert diffractometer equipped with a curved graphite monochromator applying $\text{CuK}\alpha$ ($\lambda = 0.154$ nm) radiation. Transmission electron microscopy (TEM) was performed by using JEOL 2010 microscope. The sample was dispersed in isopropanol and dropped on a copper grid coated with a carbon film. To determine the mean diameter of gold particles more than 200 particles were chosen. The mean diameter (d_m) of particles was calculated using well known procedure from histograms of particle size distribution with the following formula: $d_m = \sum_i(x_i d_i)/\sum_i x_i$, where x_i is the number of particles with diameter d_i .

X-ray photoelectron spectra were recorded using SPECS spectrometer with PHOIBOS-150 hemispherical energy analyzer and $\text{AlK}\alpha$ irradiation ($h\nu = 1486.61$ eV, 200 W). All measured binding energies (BE) were referred to C1s line of adventitious carbon at 284.8 eV. The pass energy of the analyzer was 20 eV.

In situ UV-visible (UV-vis) spectroscopic analysis of the gold species transformation under temperature-programmed reduction (TPR) was carried out in a lab made set-up [30] with simultaneous analysis of gas phase components and recording of the UV-vis spectra of the sample. Spectra were collected using an AVANTES AvaSpec-2048 UV-visible spectrometer equipped with an AvaLight-DHS light source and a high temperature optic fiber reflection probe located close to the external wall of the quartz reactor. Time of spectrum recording was about 5 ms. UV-vis spectra recorded each 15 s were obtained by subtraction of the initial spectrum recorded at room temperature from those recorded at elevated temperatures. The reactor packed with MgO was used as a reference.

Ex situ UV-vis spectroscopic analysis of the gold species transformation was carried out at room temperature using the same spectrometer and standard diffuse reflectance cell.

2.3. Hydroxymatairesinol (HMR) oxidation

Lignan HMR was extracted from ground Norway spruce knots by acetone–water mixture as described in [31]. The extract was concentrated in a rotary evaporator and then purified by flash chromatography. HMR was obtained as a mixture of two diastereomers HMR 1 and HMR 2, and the HMR 2-to-HMR 1 molar ratio was 2. The purity of HMR was determined by gas chromatography (GC) to be 95%. The major contaminants were lignans: α -conidendrin (Coni) and α -conidendric acid (ConiA), which structures are presented in Scheme 1. Both isomers, HMR 1 and HMR 2, could be oxidized, and the isomerization between them occurs as well.

The reaction was performed in a stirred 200 ml glass reactor under atmospheric pressure, equipped with a heating jacket (using silicon oil as the heat transfer medium), a re-flux condenser (cooling medium set at –20 °C), oil lock, pitched-blade turbine and stirring baffles. In a typical experiment, the catalyst was charged into the reactor in the amount corresponding to 5 mg of the active metal. The catalyst grain size was 45–63 μm to suppress the internal mass transfer limitations. Catalysts were tested using 2 vol.% propan-2-ol (Sigma-Aldrich, 99.8%) in water as a solvent, which was shown to be the most effective in one in the previous work of the authors [13]. The reactant solution (100 ml) with an HMR concentration of 1 mg/ml was poured into the reactor. Synthetic air (20% oxygen and 80% nitrogen, supplied by AGA, 99.999%) gas flow was set to be 100 ml/min. The stirring was started (1000 rpm to avoid external

mass transfer limitations) at reaction time set to zero and the first sample was withdrawn.

2.4. Product analysis

The samples withdrawn from the reactor at different time intervals were analyzed by GC (Perkin Elmer Instrumentary, Auto System XL) equipped with autosampler using a HP-1 column (length 25 m, inner diameter 0.20 mm, film thickness 0.11 μm) and a flame ionization detector (FID) operating at 300 °C. Prior to the GC analysis an internal standard containing mainly betulinol and C21:0 fatty acid was added, the solvent was evaporated and the samples were silylated. More details of the analysis procedure are given in [13]. The initial temperature of the column was 120 °C (for 1 min), and the temperature was increased at a rate 6 °C/min to 300 °C (for 10 min). The peaks were verified by analysis with a gas chromatograph–mass spectrometer (GC-MS, Hewlett Packard) applying the same GC conditions.

3. Results and discussion

3.1. Formation of Au NPs

In order to prepare Au NPs of a small size a freshly prepared $\text{Au}/\text{Al}_2\text{O}_3$ -F sample was treated by UV irradiation at room temperature, which permits to avoid agglomeration of formed metallic gold species. For the first time this technique was applied for the formation of Au NPs in HAuCl_4 aqueous solutions in [32]. Later on ultraviolet irradiation was used for the formation of metallic gold species supported on titania [33]. In the current study it was anticipated that gold hydroxide being supported on alumina [37] may also be reduced into Au NPs via ionization of pre-adsorbed water under ultraviolet irradiation [34]. The formation of Au NPs under UV irradiation was monitored by UV-vis spectroscopy ex situ. The presence of metallic gold species could be easily detected by the appearance of well resolved plasmon peak at the wavelength of ca. 530 nm in the UV-visible spectrum, which is characteristic for metal gold NPs [35–37]. It was observed, that the freshly prepared $\text{Au}/\text{Al}_2\text{O}_3$ -F catalyst did not contain supported metallic gold species. UV-visible spectra obtained after different time of treatment of $\text{Au}/\text{Al}_2\text{O}_3$ -F catalyst are presented in Fig. 1 (left). After the first hour of treatment by UV irradiation the peak of plasmon appeared, which was associated with the initiation of metal Au particles formation. The dependence of the plasmon peak intensity and position on time of treatment is presented in Fig. 1 (right). Since the intensity of the plasmon peak was not changing after 10 h of the catalyst treatment by UV irradiation the formation of Au NPs can be considered to be complete by this time. According to a theoretical estimation described in [38] the observed blue shift of the peak position under the sample treatment by UV irradiation corresponds to the Au NPs growth in media with a dielectric constant below 3, such as air. It implies that Au NPs were predominantly formed via the attack of the external surface of gold hydroxide particles with solvated electrons [34] yielded by the ionization of pre-adsorbed water. The catalyst treated by UV irradiation for 12 h was denoted as $\text{Au}/\text{Al}_2\text{O}_3$ -UV.

In order to form larger Au NPs of various sizes, the freshly prepared $\text{Au}/\text{Al}_2\text{O}_3$ -F was exposed to the thermal treatment in hydrogen flow at different temperatures (250–600 °C). The catalyst treatment at 600 °C was conducted for extended period of time such as 16 and 168 h to further increase particle size. The UV-vis spectroscopy in situ was applied to monitor the formation of Au NPs. The spectra obtained are presented in Fig. 2 (left). The appearance of the plasmon peak in UV-vis spectra at temperatures above 50 °C manifested the start of the Au NPs formation (Fig. 2, left,

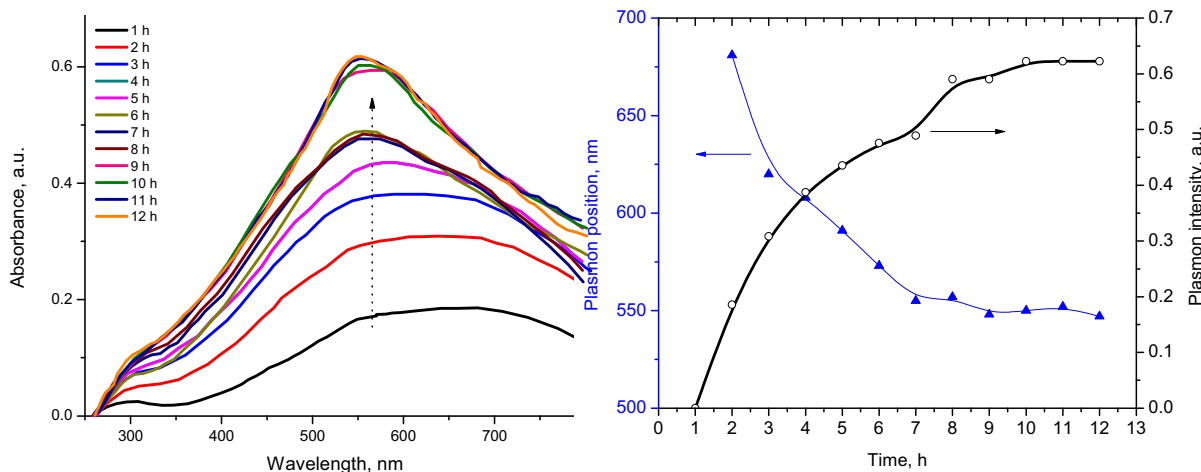


Fig. 1. Ex situ UV-visible spectra of $\text{Au}/\text{Al}_2\text{O}_3$ catalyst under UV irradiation at 254 nm vs time (left). Intensity and position of the plasmon peak vs treatment temperature (right).

marked with a white arrow). The changes of normalized intensity and position of plasmon peak with temperature of thermal treatment are presented in Fig. 2 (right). The plasmon peak intensity almost reached its maximum at about 250 °C. In contrast to the formation of Au NPs under UV irradiation, thermal treatment led to the red shift of plasmon peak within the temperature interval 50–250 °C. Such shift of the plasmon peak corresponds to the formation of Au NPs initially inside of gold hydroxide particles due to their sequential thermal decomposition: $\text{Au}(\text{OH})_3 \rightarrow \text{Au}_2\text{O}_3 \rightarrow \text{Au}$ [39]. The sample obtained at 250 °C was denoted as $\text{Au}/\text{Al}_2\text{O}_3$ -250 and selected for the catalytic test. Further thermal treatment of the formed Au NPs resulted in the blue shift of the plasmon peak for the temperature interval 250–350 °C. Since the media surrounding supported Au NPs is characterized with the dielectric constant for air (ca. 1), the plasmon peak shift was associated with agglomeration of supported Au NPs. Therefore, sample obtained at 350 °C was selected for further catalytic tests and was denoted as $\text{Au}/\text{Al}_2\text{O}_3$ -350. At temperatures above 500 °C some changes in the shape of plasmon peak were observed. Intensity of the peak shoulder at high wavelengths decreased with an increase of temperature (Fig. 2, left). The latter may be assigned to the disappearance of small Au NPs interaction between *inter se* due to their agglomeration as it was noted in [40,41]. Thus, other samples for catalytic tests were obtained by thermal treatment at 600 °C for 16 h or for 168 h

(7 days) and were denoted as $\text{Au}/\text{Al}_2\text{O}_3$ -600-16 h and $\text{Au}/\text{Al}_2\text{O}_3$ -600-168 h, respectively.

The Au NPs found by TEM in the studied samples (dark features marked with arrows) were characterized with almost spherical shape practically without any well detectable crystallographic planes (Fig. 3). Metallic Au NPs were observed in TEM images for the as-prepared sample, although those particles were not detected by UV-vis. Most likely Au NPs were formed as a result of gold hydroxide decomposition/reduction under the sample evacuation in the microscope vacuum chamber and/or due to the sample exposure to the electron beam. The size of Au NPs for $\text{Au}/\text{Al}_2\text{O}_3$ -F sample seemed to be determined by the size of initial $\text{Au}(\text{OH})_3$ particles deposited on the alumina during the preparation. Analysis of TEM images showed that the average size of Au NPs in $\text{Au}/\text{Al}_2\text{O}_3$ -F (Fig. 3A) and $\text{Au}/\text{Al}_2\text{O}_3$ -UV (Fig. 3F) was found to be similar, ca. 1.8–1.9 nm. It was confirmed that conditions of UV-radiation did not cause agglomeration of the primary deposited Au species, although thermal treatment of catalysts at temperatures of 250–600 °C resulted in the variations in Au NPs size (see Table 1). The mean diameter of Au NPs prepared by catalyst treatment at 250 °C ($\text{Au}/\text{Al}_2\text{O}_3$ -250) was ca. 3 nm (Fig. 3B). Increase of the treatment temperature by 100 °C resulted in a slight increase of Au NPs size up to 3.2 nm in $\text{Au}/\text{Al}_2\text{O}_3$ -350 (Fig. 3C), while an increase of treatment temperature up to 600 °C as well as increasing time

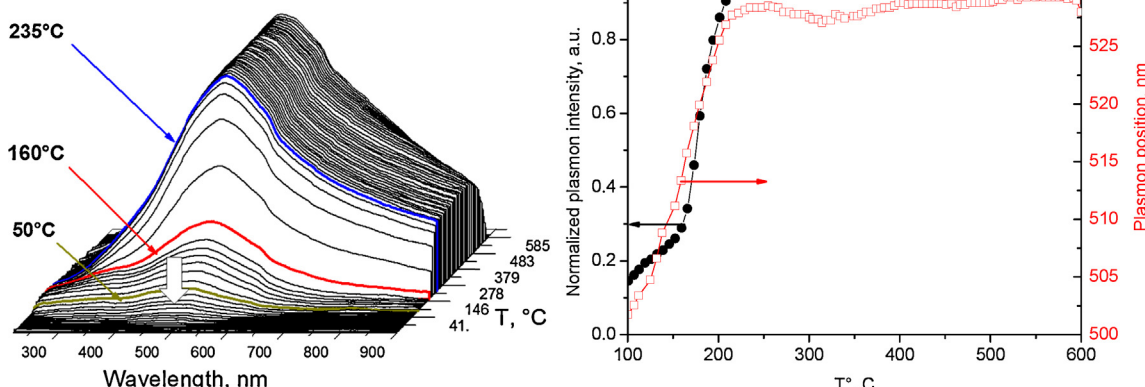


Fig. 2. In situ UV-visible spectra of $\text{Au}/\text{Al}_2\text{O}_3$ catalyst under thermal treatment in hydrogen with a temperature ramp rate 20 °C/min (left). Normalized intensity and position of the plasmon peak vs. treatment temperature (right).

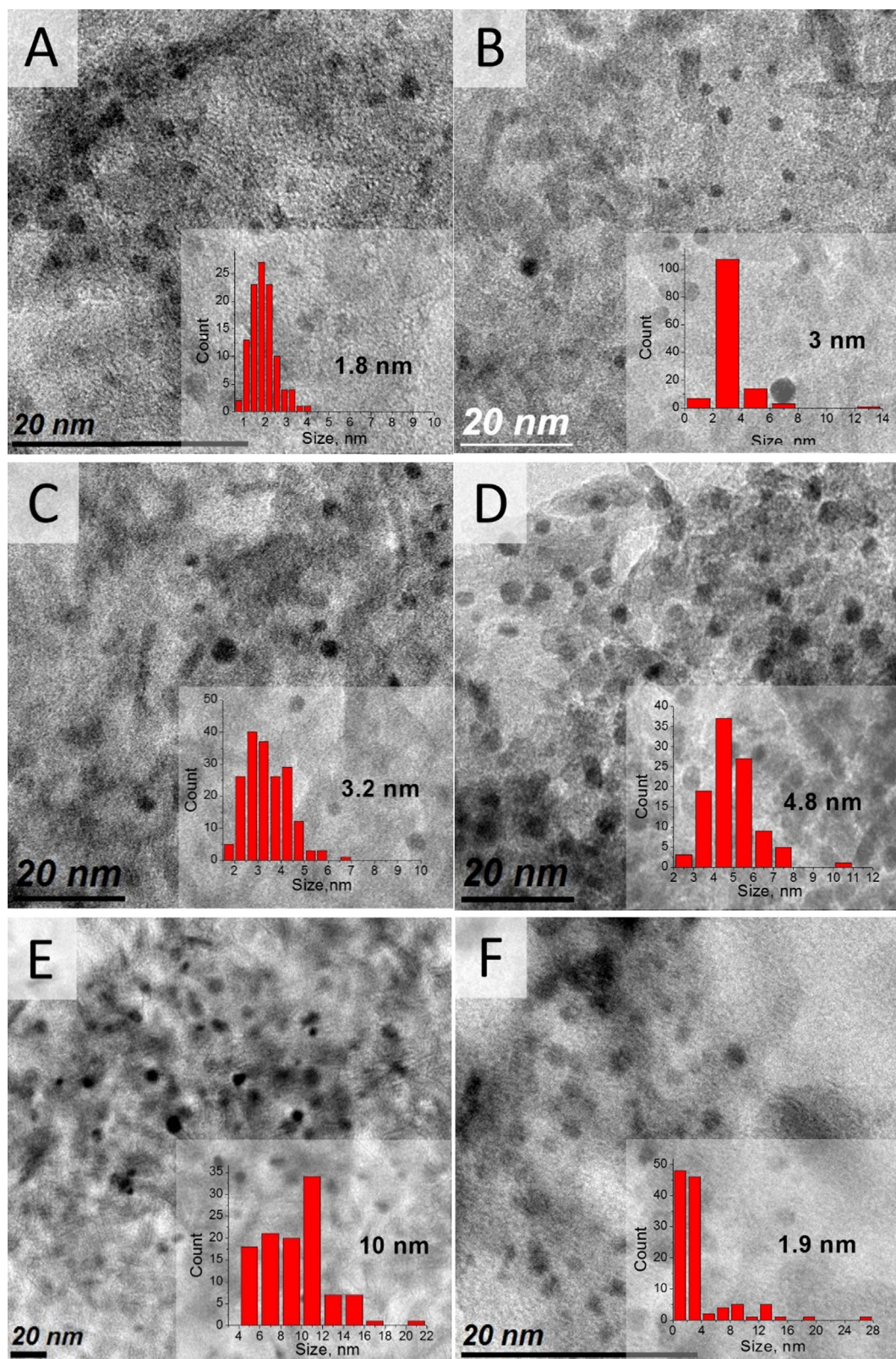


Fig. 3. TEM micrographs and histograms of gold nanoparticles size distribution for Au/Al₂O₃ sample: A – fresh sample after drying (Au/Al₂O₃-F); B – thermally treated at 250 °C (Au/Al₂O₃-250); C – thermally treated at 350 °C (Au/Al₂O₃-350); D – thermally treated at 600 °C for 16 h (Au/Al₂O₃-600-16 h); E – thermally treated at 600 °C for 168 hours (Au/Al₂O₃-600-168 h); F – treated by UV irradiation at 254 nm during 12 h (Au/Al₂O₃-UV).

Table 1

Average size of the supported Au NPs according to TEM analysis.

Catalyst	Average Au particle size (nm)
Au/Al ₂ O ₃ -F	1.8 ± 0.6
Au/Al ₂ O ₃ -UV	1.9 ± 1.1
Au/Al ₂ O ₃ -250	3.0 ± 1.3
Au/Al ₂ O ₃ -350	3.2 ± 0.9
Au/Al ₂ O ₃ -600-16 h	4.8 ± 1.2
Au/Al ₂ O ₃ -600-168 h	10.0 ± 3.2

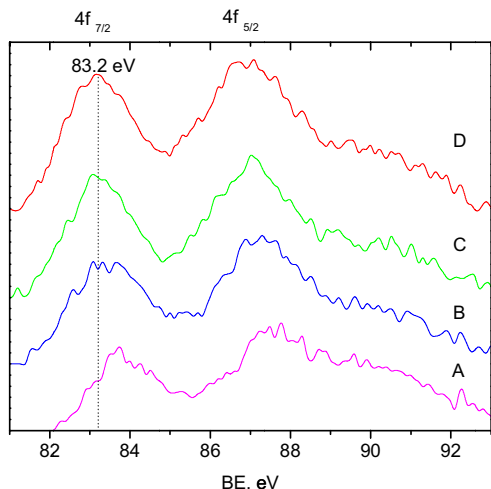


Fig. 4. A4 4f XP spectra of Au/Al₂O₃ catalysts prepared by treatment under UV irradiation at 254 nm during 12 h – Au/Al₂O₃-UV (A) or in hydrogen at 250 °C – Au/Al₂O₃-250 (B), at 350 °C – Au/Al₂O₃-350 (C); at 600 °C – Au/Al₂O₃-600 (D).

of the treatment to 16 h (Au/Al₂O₃-600-16 h) or 168 h (Au/Al₂O₃-600-168 h) significantly affected the size of Au NPs (Fig. 3D and E).

The chemical state of the gold species formed on the surface of the obtained catalysts was characterized by XPS technique. The XPS spectra for Au 4f region are presented in Fig. 4. All spectra were characterized by one doublet of two spin-orbit components separated by 3.67 eV, i.e., Au 4f_{7/2} and Au 4f_{5/2}. The curve fitting

of spectra Au 4f indicates Au 4f_{7/2} components at BE value around 83.2–83.5 eV, which can be attributed to Au⁰ species in accordance to [42,43]. Some variations of peak position seem to be caused by the presence of organic residuals on the alumina prepared from an organo-metallic precursor.

3.2. Hydroxymatairesinol (HMR) oxidation

3.2.1. Catalyst activity

Gold catalysts with different Au particle size (1.9–10 nm) were evaluated in HMR selective oxidation. The obtained dependence of oxoMAT concentration changes on time over catalysts with different particle sizes is presented in Fig. 5. The highest activity was achieved over gold clusters of 3.2 nm (Au/Al₂O₃-350), while the catalyst with the smallest gold particles (1.9 nm) demonstrated zero activity (Au/Al₂O₃-UV).

Experiments were carried out several times to confirm reproducibility of the obtained values. Catalytic activity defined as the initial rate within 10 min was found to be dependent on the gold cluster size and have a volcano relationship with the particle size (Fig. 6). The values of initial rate were estimated taking into account standard deviations for particle size (shown in Table 1) and errors for the detection of the initial reagents and formed products by gas chromatographic analysis (3–5%). The highest activity was achieved over gold clusters of ca. 4 nm.

It is important to emphasize that the reaction rate in the current work at maximum is four fold higher than in the case of gold catalysts supported on commercial γ -alumina [28]. As was already mentioned, higher catalytic activity is attributed to the presence of the stronger Lewis acid sites on the prepared alumina surface [14]. Another difference between the current work with sol-gel alumina and the previous HMR selective oxidation reaction investigated in [28] with Au/ γ -Al₂O₃ is that in the latter the maximum of the reaction rate was observed with Au particle size of ca. 2 nm [28]. Therefore, there is a clear connection between the position of the rate maxima and the values of kinetic parameters.

The analysis of structure sensitivity in the case of HMR oxidation is rather complex due to involvement of the support. As was proposed before [14], metal oxide surface groups play an important role in the coordination of bulky HMR molecule (ca. 1.5 nm)

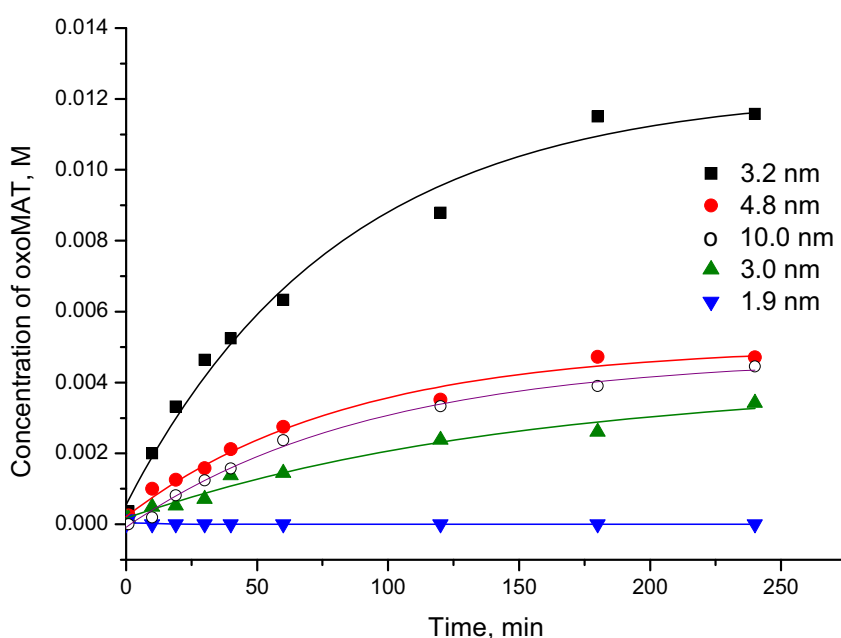


Fig. 5. Dependence of oxoMAT concentration on time over Au/Al₂O₃ catalysts.

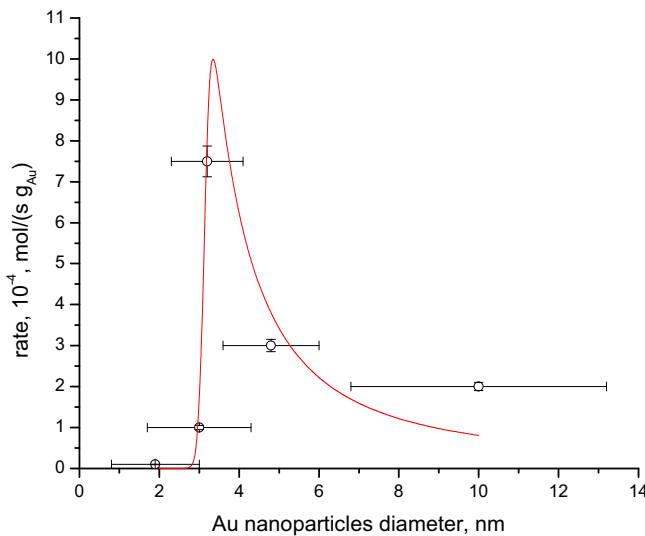


Fig. 6. Dependence of initial rates in the lignan hydroxymatairesinol selective oxidation on Au particle size of $\text{Au}/\text{Al}_2\text{O}_3$ catalyst: experimental data (squares), estimated curve (solid line).

suitable for further transformation of the lignan over gold catalysts. This step is considered to be essential for the HMR transformation. Once the molecule is in the right position, oxidation or in fact oxidative dehydrogenation [44] proceeds rapidly, enhanced by the presence of activated oxygen.

Whatever is the chemical explanation behind the structure sensitivity it is possible to apply a phenomenological thermodynamic approach to model the experimental data. Such approach is based on the differences in adsorption strength on small and large clusters due to changes in the fraction of terraces, edges and corners with the size increase [45].

It was also clearly demonstrated in [45] that position of the maximum in TOF, if there is such a maximum, depends on the values of rate parameters, such as kinetic constants, as well as the value of the Polanyi parameter and the magnitude of the difference between Gibbs energy of reactant adsorption on edges and terraces.

The kinetic model for description of the rate dependence in HMR oxidation was developed in [28] giving in the case of experimentally observed zero in oxygen and fractional order in HMR the following rate equation

$$r = \frac{p_1 e^{p_2 p_3 / d_{\text{cluster}}}}{(1 + p_4 e^{p_3 / d_{\text{cluster}}}) d_{\text{cluster}}} \quad (1)$$

with

$$p_1 = k K_{\text{HMR}} C_{\text{HMR}}, p_2 = \alpha, p_3 = \chi_{\text{HMR}}, p_4 = K_{\text{HMR}} C_{\text{HMR}} \quad (2)$$

where k is the modified rate constant of rds , K_{HMR} and C_{HMR} are the adsorption constant of HMR on terraces and concentration of HMR, respectively, α is the Polanyi parameter of rds , χ is the difference between Gibbs energy of HMR adsorption on edges and terraces divided by RT .

Comparison of experimental data with the calculations showed rather good correspondence of them (Fig. 6). A model describing volcano-shape dependence of the turnover-frequency on the Au particle size has the maximum of catalytic activity corresponding to the Au particle with diameter of ca. 3.5–4 nm. The values of the parameters could not have been identified with certainty due to a limited set of data. Analysis of the position maximum can be used in principle to improve statistical identification of the parameters, as in certain cases position of the rate maximum can be theoretically determined by analyzing the derivative of the reciprocal function of the reaction rate [46]. However, such analysis cannot be easily done

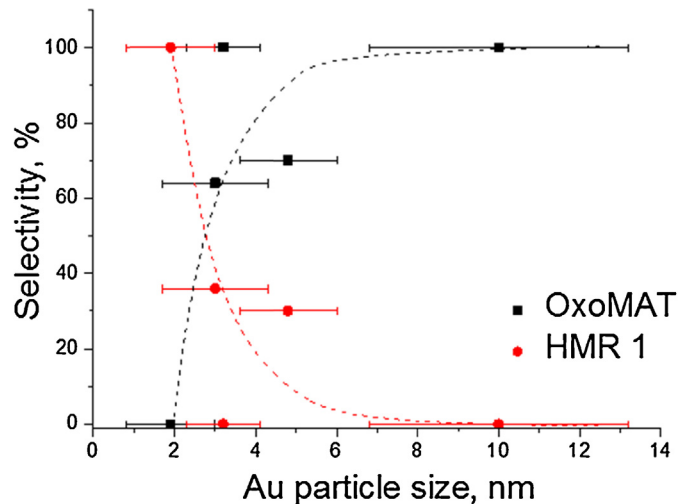


Fig. 7. Dependence of selectivity in the lignan hydroxymatairesinol (HMR) selective oxidation to oxomatairesinol (oxoMAT) on Au particle size of $\text{Au}/\text{Al}_2\text{O}_3$ catalyst.

for Eq. (1) requiring Taylor expansion of exponential functions. In any case difference in the location of the rate maximum can be attributed to the values of Polanyi parameter, kinetic parameters p_1 and p_4 as well as the parameter p_3 . The latter reflects the magnitude of so-called heterogeneity of gold clusters, which is related to the differences in the strength of HMR adsorption on edges and terraces for gold clusters supported on sol-gel and commercial γ -alumina. For example if due to changes in the support and interactions with it, smaller gold clusters adsorb HMR differently on sol-gel alumina and commercial γ -alumina it is natural to expect changes in the position of the rate maxima. This is a conclusion of general validity not only related to HMR oxidative hydrogenation.

3.2.2. Product distribution

There are two competitive reactions during the transformation of HMR over gold catalysts, namely oxidation of HMR and isomerization of diastereomers HMR 2 to HMR 1. The former one is typically performed over the alumina surface even in the absence of Au particles. However, in the presence of Au particles on the support surface the oxidation reaction influence is dominating [13]. Therefore, transformation of HMR over catalysts demonstrating low oxidation activity is typically resulting in the formation of both, isomerization and oxidation products. Selectivity toward HMR 1 and oxoMAT dependence on gold particles size is given in Fig. 7. Fig. 7 clearly shows that selectivity to OxoMAT is increasing with an increase of the cluster size. It was also observed, that the most active catalysts with Au particles size of 3.2 nm ($\text{Au}/\text{Al}_2\text{O}_3$ -350) and 10 nm ($\text{Au}/\text{Al}_2\text{O}_3$ -600-168 h), respectively, had 100% selectivity to oxoMAT, while the selectivity to oxoMAT of less active catalysts ($\text{Au}/\text{Al}_2\text{O}_3$ -250 and $\text{Au}/\text{Al}_2\text{O}_3$ -600-16 h) was lower.

4. Conclusions

The synthesis of supported Au which allows control of Au NPs particle size was applied. The growth of the Au particles under influence of UV irradiation and temperature was thoroughly investigated. The reaction structure sensitivity of the selective oxidation of the lignan hydroxymatairesinol (HMR) over gold catalysts was demonstrated. A model was developed describing volcano-shape dependence of the turnover-frequency on the Au particle size, where the maximum of catalytic activity was corresponding to the Au particle diameter of ca. 4 nm.

References

- [1] M. Haruta, T. Kobayashi, H. Sano, N. Yamada, *Chem. Lett.* 16 (1987) 405–408.
- [2] G.J. Hutchings, *J. Catal.* 96 (1985) 292–295.
- [3] B. Nkosi, N.J. Coville, G.J. Hutchings, *Appl. Catal.* 43 (1988) 33–39.
- [4] A. Mirescu, U. Prüßé, *Appl. Catal. B* 70 (2007) 644.
- [5] Y. Román-Leshkov, J.N. Chheda, J.A. Dumesic, *Science* 312 (2006) 1933.
- [6] C.H. Christensen, B. Jørgensen, J. Rass-Hansen, K. Egeblad, R. Madsen, S.K. Klitgaard, S.M. Hansen, M.R. Hansen, H.C. Andersen, A. Riisager, *Angew. Chem. Int. Ed.* 45 (2006) 4648.
- [7] B. Jørgensen, S.E. Christiansen, M.L.D. Thomsen, C.H. Christensen, *J. Catal.* 251 (2007) 332.
- [8] Z. Martinez-Ramirez, S.A. Jimenez-Lam, L.C. Fierro-Gonzalez, *J. Mol. Catal. A* 344 (2011) 47.
- [9] A. Corma, H. Garcia, *Chem. Soc. Rev.* 37 (2008) 2096–2126.
- [10] F. Kawamura, M. Miyachi, S. Kaway, *J. Wood Sci.* 44 (1998) 47.
- [11] P. Eklund, A. Lindholm, J.-P. Mikkola, A. Smeds, R. Lehtilä, R. Sjöholm, *Org. Lett.* 5 (4) (2003) 491.
- [12] H. Markus, A.J. Plomp, T. Sandberg, V. Nieminen, J.H. Bitter, D.Yu. Murzin, *J. Mol. Catal. A* 274 (2007) 42.
- [13] O.A. Simakova, E.V. Murzina, P. Mäki-Arvela, A.-R. Leino, B.C. Campo, K. Kordas, S. Willför, T. Salmi, D.Yu. Murzin, *J. Catal.* 282 (2011) 54.
- [14] O.A. Simakova, E. Smolentseva, M. Estrada, E.V. Murzina, S. Beloshapkin, S.M. Willför, A.V. Simakov, D.Yu. Murzin, *J. Catal.* 291 (2012) 95–103.
- [15] G.C. Bond, D.T. Thompson, *Catal. Rev. Sci. Eng.* 41 (1999) 319.
- [16] N. Lopez, T.V.P. Janssens, B.S. Claussen, Y. Xu, M. Mavrikakis, T. Bligaard, J.K.N. Ørskov, *J. Catal.* 223 (2004) 232.
- [17] B. Hvolbæk, T.V.W. Janssens, B.S. Claussen, H. Falsig, C.H. Christensen, J.K.N. Ørskov, *Nanotoday* 2 (2007) 14.
- [18] F. Bocuzzi, A. Chiorino, S. Tsubota, M. Haruta, *J. Phys. Chem. B* 100 (1996) 3625.
- [19] S. Miscino, S. Scire, C. Crisafulli, A.M. Visco, S. Galvagno, *Catal. Lett.* 44 (1997) 273.
- [20] A. Sanchez, S. Abbet, U. Heiz, W.-D. Schneider, H. Hakkinen, R.N. Barnett, U. Landman, *J. Phys. Chem. A* 103 (1999) 9573.
- [21] Y. Xu, M. Mavrikakis, *J. Phys. Chem. B* 107 (2003) 690.
- [22] X.-F. Yang, A.-Q. Wang, Y.-L. Wang, T. Zhang, J. Li, *J. Phys. Chem. C* 114 (2010) 3131.
- [23] M. Valden, S. Pak, X. Lai, D.W. Goodman, *Catal. Lett.* 56 (1998) 7.
- [24] S. Demirel-Gülen, M. Lucas, P. Claus, *Catal. Today* 102–103 (2005) 166.
- [25] Y. Guan, E.J.M. Hensen, *Appl. Catal. A* 361 (2009) 49.
- [26] Y. Önal, S. Schimpf, P. Claus, *J. Catal.* 223 (2004) 122.
- [27] O.A. Simakova, B.T. Kusema, B.C. Campo, A.-R. Leino, K. Kordas, V. Pitchon, P. Mäki-Arvela, D. Yu Murzin, *J. Phys. Chem. C* 115 (2011) 1036.
- [28] O.A. Simakova, E.V. Murzina, D. Yu Murzin, C. R. Chim. 17 (2014) 770–774.
- [29] G. Perez, S. Fuentes, V. Petranovskii, A. Simakov, *Catal. Lett.* 110 (2006) 53–60.
- [30] B. Acosta, E. Smolentseva, S. Beloshapkin, R. Rangel, M. Estrada, S. Fuentes, A. Simakov, *Appl. Catal. A: Gen.* 449 (2012) 96–104.
- [31] S.M. Willför, M.O. Ahotupa, J.E. Hemming, M.H.T. Reunananen, P.C. Eklund, R.E. Sjöholm, C.S.E. Eckerman, S.P. Pohjamo, B.R. Holmbom, *J. Agr. Food Chem.* 51 (2003) 7600.
- [32] S. Dong, C. Tang, H. Zhou, H. Zhao, *Gold Bull.* 37 (3–4) (2004) 187.
- [33] M. Yang, L.F. Allard, M. Flytzani-Stephanopoulos, *J. Am. Chem. Soc.* 135 (2013) 3768–3771.
- [34] J. Belloni, *Catal. Today* 113 (2006) 141–156.
- [35] W. Chen, J. Zhang, W. Cai, *Scr. Mater.* 48 (2003) 1061–1066.
- [36] C. Lopez-Bastida, E. Smolentseva, V. Petranovskii, R. Machorro, *Plasmon. Springer* 8 (2013) 1551–1558.
- [37] E. Smolentseva, A. Simakov, S. Beloshapkin, M. Estrada, E. Vargas, V. Sobolev, R. Kenzhin, S. Fuentes, *Appl. Catal. B: Environ.* 115–116 (2012) 117–128.
- [38] I. Tuzovskaya, N. Bogdanchikova, A. Simakov, V. Gurin, A. Pestyakov, M. Avalos, M. Farías, *Chem. Phys.* 338 (2007) 23–32.
- [39] V.V. Costa, M. Estrada, Yu. Demidova, I. Prosvirin, V. Kriventsov, R.F. Cotta, S. Fuentes, A. Simakov, E.V. Gusevskaya, *J. Catal.* 292 (2012) 148–156.
- [40] C.L. Nehla, J.H. Hafner, *J. Mater. Chem.* 18 (2008) 2415–2419.
- [41] I. Tuzovskaya, N. Bogdanchikova, A. Simakov, V. Gurin, A. Pestyakov, M. Avalos, M.H. Farias, *Chem. Phys.* 338 (2007) 23–32.
- [42] J.F. Moulder, W.F. Stickle, P.E. Sobol, K.D. Bomben, *Handbook of X-ray Photoelectron Spectroscopy*, Perkin-Elmer Corporation, Physical Electronics Division, Eden Prairie, 1992, pp. 179.
- [43] A.M. Visco, F. Neri, G. Neri, A. Donato, C. Milone, S. Galvagno, *Phys. Chem. Chem. Phys.* 1 (1999) 2869–2873.
- [44] A. Prestianni, F. Ferrante, O.A. Simakova, D. Duca, D.Yu. Murzin, *Chem. Eur. J.* 19 (2013) 4577–4585.
- [45] D.Yu. Murzin, *J. Catal.* 276 (2010) 85.
- [46] M.I. Temkin, *Kinet. Katal.* 25 (1984) 299.